Solar Energy Materials & Solar Cells 120 (2014) 591–595

Contents lists available at ScienceDirect

Solar Energy Materials & Solar Cells

journal homepage: www.elsevier.com/locate/solmat

Plasmonic-enhanced Si Schottky barrier solar cells

Chong Tong, Juhyung Yun, Haomin Song, Qiaoqiang Gan *, Wayne A. Anderson *

Department of Electrical Engineering, The State University of New York at Buffalo, Buffalo, NY 14260-1920, USA

ARTICLE INFO

Article history:
Received 30 May 2013
Received in revised form
24 September 2013
Accepted 2 October 2013
Available online 30 October 2013

Keywords:
Plasmonic-enhanced
Nanoparticles
Tunable light trapping effect

ABSTRACT

By introducing silver nanoparticles (NPs) and SiO_2 spacer layers on top of Si-based Schottky barrier solar cells, we demonstrated a positive and tunable light trapping effect introduced by metallic NPs. A redshift of the surface plasmon resonant wavelength of Ag NPs from 550 nm to 650 nm, corresponding to the optical absorption peak of the solar cell, was observed with an increased average particle diameter from 19.7 nm to 85 nm. Enhanced light trapping effects at distinct resonance wavelengths were observed in the optical spectra of the plasmonic-enhanced devices. Electrical measurements confirmed the expected photocurrent improvement at these corresponding wavelengths. It was also revealed that the Ag NPs enhance the carrier generation rate inside of the Si active layer without sacrificing carrier collection efficiency of the device. The short-circuit current density of the best cell we obtained in this work was improved from 13.7 mA/cm^2 to 19.7 mA/cm^2, with an enhancement factor of 43.7%.

1. Introduction

Schottky barrier solar cells have received intensive research due to their simple, low-temperature and low-cost fabrication process, the adaptability to polycrystalline thin film devices and the potential to achieve high power conversion efficiencies [1–3]. However, because of the inherent metal–insulator–semiconductor (MIS) structure, the reflection and absorption of the composite metallic surface are still significant even by adding an antireflection coating on top of the device [1,4]. Achieving high optical transmission through the top metal surface into the semiconductor absorber layer still remains challenging, limiting the short-circuit current density (J_{sc}) of the MIS Schottky barrier solar cells [1]. Recently, plasmonic enhancement using metallic nanoparticles (NPs) offered new opportunities to engineer and improve the performance of photo-harvesting devices, such as photodetectors [5–8] and solar cells [9–13]. By controlling the shape, size, distribution and surrounding dielectric environment of metallic NPs, the surface plasmon resonant wavelength (λ_{SPR}) can be tuned to desired spectral regions [14]. It is generally believed that large size NPs (e.g., >50 nm in diameter) can provide stronger plasmonic scattering intensities and higher scattering/absorption cross-sections [15]. However, the scattering effects are primarily restricted to a limited range of scattering angles [16]. In contrast, relatively small NPs (e.g., <50 nm diameter) can result in stronger near-field localized field enhancement [17,18] and then scatter the light into a broader range of angles [15]. Unfortunately, smaller metallic NPs are usually associated with more significant detrimental light absorption in particles [9,10]. Therefore, to achieve optimized optical absorption enhancement in semiconductor active layers, the size of NPs needs to be tailored for different device applications and structures.

In this paper, we introduce silver (Ag) NPs and silicon dioxide (SiO_2) spacer layers on top of a Si MIS Schottky barrier solar cell. The size and distribution of the Ag NPs are tuned to enhance the optical absorption in the Si absorber layer and thereby improve the overall performance of the device.

2. Experimental section

A Si MIS Schottky solar cell with Ag NPs on top of a thin SiO_2 spacer layer is illustrated schematically in Fig. 1. There are two-fold effects by inserting this thin spacer layer between NPs and the Si Schottky solar cell device: (1) the λ_{SPR} of Ag NPs can be tuned to the visible wavelength range due to the change of the local dielectric environment [19], and (2) an electrical isolation can be formed to avoid additional surface recombination owing to the presence of the metal particles [20]. The Ag NPs are formed by annealing the Ag thin film deposited on top of the spacer layer at a moderate temperature of 200 °C. The size distribution of these NPs can be adjusted by controlling thicknesses of the Ag thin films, which were deposited via thermal evaporation (Denton Vacuum, DV-502). This nanoparticle formation technique is suitable for practical large-scale implementation and it also allows us to easily tune the characteristics of the NPs to achieve device enhancement. More details about these Ag NPs were discussed elsewhere in our

* Corresponding authors.
E-mail addresses: qqgan@buffalo.edu (Q. Gan), waanders@buffalo.edu (W.A. Anderson).

0927-0248/$ - see front matter © 2013 Elsevier B.V. All rights reserved.
http://dx.doi.org/10.1016/j.solmat.2013.10.001

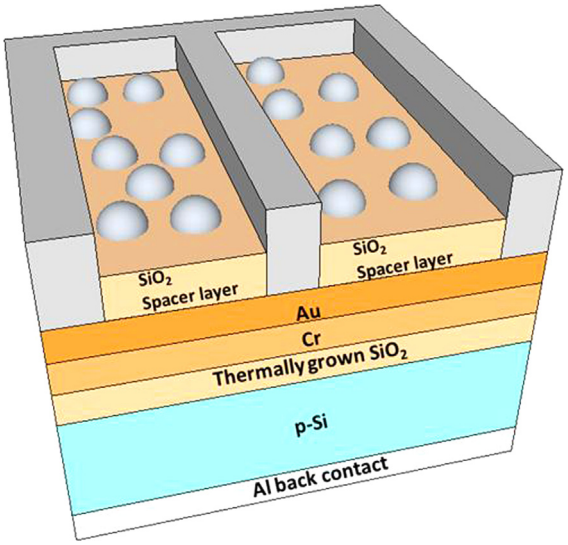

Fig. 1. A schematic illustration of the proposed plasmonic-enhanced Si Schottky barrier solar cell.

recent work [21]. As shown in Fig. 1, the Si Schottky barrier solar cell has a typical structure of Ag grid/Au/Cr/SiO_2/p-Si substrate/Al back contact. The p-Si wafer was etched in buffered HF, cleaned in deionized water, dried in N_2, and placed in a 10^{-6} Torr vacuum system for the Al back contact deposition. Then, the wafer was heated to 600 °C in air to form the Ohmic contact between p-Si and Al, and form a ~20 Å thermally grown SiO_2 layer over the exposed area on top of the Si wafer, followed by the deposition of a ~60 Å-thick Cr film for the Schottky barrier and a ~70 Å-thick Au film to reduce the sheet resistance and work as an oxidation barrier, simultaneously. The spacer layer of SiO_2 with desired thickness was deposited on top of the device by a PECVD reactor (Plasma System 100, Oxford Instruments), followed by forming NPs on the top. The thickness and the refractive index of the spacer layer were measured by an ellipsometer (Gaertner Scientific) to be 40 nm and $n=1.46$ at 633 nm. In this work, we prepared four different devices for comparison, including (1) a reference cell with no NPs or spacer layer, (2) a cell with a spacer layer only, and two cells with NPs formed by (3) a 5-nm-thick Ag film and (4) a 15-nm-thick Ag film.

The deposited Ag NPs were characterized by scanning electron microscopy (SEM). All solar cell devices were characterized under room temperature. The photocurrent was analyzed using a solar simulator under the AM 1.5G illumination condition. The reflectance spectra were characterized using a spectral ellipsometer (J.A. Wollam, V-Vase). For the external quantum efficiency (EQE) measurement, a monochromatic light was extracted from a quartz tungsten halogen lamp and focused onto the devices. The light power was measured using a calibrated silicon photodetector (FDS-1010CAL, Thorlabs).

3. Results and discussion

The SEM images for the Ag NPs formed on sample 3 and sample 4 are shown in Fig. 2(a) and (c), respectively. The randomly distributed NPs were formed due to the surface tension of Ag thin films [9]. These Ag NPs provide different surface plasmon resonances depending on their sizes, shapes and distributions. One can see from Fig. 2(a) that those Ag NPs annealed from a 5-nm-thick Ag thin film on sample 3 are generally spherical. While for sample 4 shown in Fig. 2(c), larger Ag NPs annealed from a 15-nm-thick Ag film have a combination of oblate and sphere shapes. More quantitatively, we plot the extracted size distributions of these particles in Fig. 2(b) and (d). One can see that larger NPs (with an average diameter of 85.0 nm) on sample 4 have a much larger standard deviation of 33 nm compared with the 6.2 nm for the smaller NPs (with an average diameter of 19.7 nm) on sample 3, covering a broader size distribution. The surface coverage of NPs is 36.7% on sample 3, which is similar to that of sample 4 (i.e., 33.7% coverage).

To evaluate the light trapping effect introduced by these NPs, we characterize the angle-dependent reflection spectra for different incident angles from 20° to 60° in the wavelength range from 400 nm to 1000 nm, as shown in Fig. 3(a)–(d). Compared with the reference cell (see Fig. 3(a)), the surface reflection of the cell with a spacer layer was depressed in a broad wavelength range from 400 nm to 1000 nm due to the anti-reflection effect of the SiO_2 spacer layer, as shown in Fig. 3(b). After introducing Ag NPs on top of the spacer layer, reflectance for samples 3 and 4 were further decreased, indicating the enhanced light trapping effect contributed by these Ag NPs. Obvious reflectance dips corresponding to surface plasmon resonant wavelengths of these NPs were observed, as shown in Fig. 3(c) and (d). A red shift of the reflectance dip from ~550 nm (indicated by the dashed line in Fig. 3(c)) to ~650 nm (indicated by the dashed line in Fig. 3(d)) can be observed, demonstrating the spectral shift of the surface plasmon resonance for different sized Ag NPs. With larger particle size and deviation, the red-shifted surface plasmon resonance is broader as shown in Fig. 3(d), resulting in a much wider reflectance dip for sample 4, which is highly desired for improved device performance [20,22].

For a photovoltaic device, it is essential to determine whether the improved light trapping effect can contribute to the photogenerated current. According to our measurement, the short-circuit current density J_{sc} is 13.7 mA/cm^2 for the reference sample 1 in Fig. 3(a). For sample 2 with the spacer layer only (see Fig. 3(b)), the J_{sc} was increased to 17.6 mA/cm^2 due to the anti-reflection effect of the SiO_2 spacer layer. For samples 3 and 4, the J_{sc} values were further improved to 18.4 mA/cm^2 and 19.7 mA/cm^2, respectively, indicating the extra optical absorption enhancement of the active Si layer contributed by those Ag NPs shown in Fig. 2. To confirm the light trapping enhancement, we plot the measured EQE of each cell in Fig. 4. Compared with the reference cell (see black dots in Fig. 4), the EQE of the cell with the spacer layer only (i.e., sample 2, see red empty circles) was enhanced in a very broad wavelength range due to the surface reflectance depression effect of the spacer layer, resulting in an photocurrent enhancement of 28.5%. The EQE peak corresponding to the maxima of these two absorption spectra was not shifted in this case. For plasmonic-enhanced solar cells with Ag NPs on top of spacer layers, broadband enhancements were observed from 500–550 nm to 1000 nm (see empty triangular dots in Fig. 4, corresponding to samples 3 and 4), resulting in an overall photocurrent enhancement of 34.3% and 43.7%, respectively, owing to the enhanced forward scattering of Ag NPs into the high refractive index active layers. The reduction at shorter wavelength in the spectral range from 400 to 500–550 nm is mainly due to the backscattering and dissipation in Ag NPs below their surface plasmon resonant wavelengths [23]. One can see that the EQE peak locations of these two plasmonic-enhanced solar cells (i.e., sample 3 and 4) were shifted from 550 nm to 650 nm and perfectly matched with the shift of surface plasmon resonance wavelengths shown in Fig. 3(c) and (d). This close correspondence between plasmon resonances and EQE spectra is a clear evidence to demonstrate the role of plasmonic effect in the observed photocurrent enhancement.

Particularly, the best cell we obtained in this work is the one with Ag NPs formed from a 15-nm-thick Ag film (i.e., sample 4). As shown in Fig. 3(d), an omnidirectional low reflection ($<10\%$) was obtained up to 60° of the incident angle in the wavelength range of 500–800 nm.

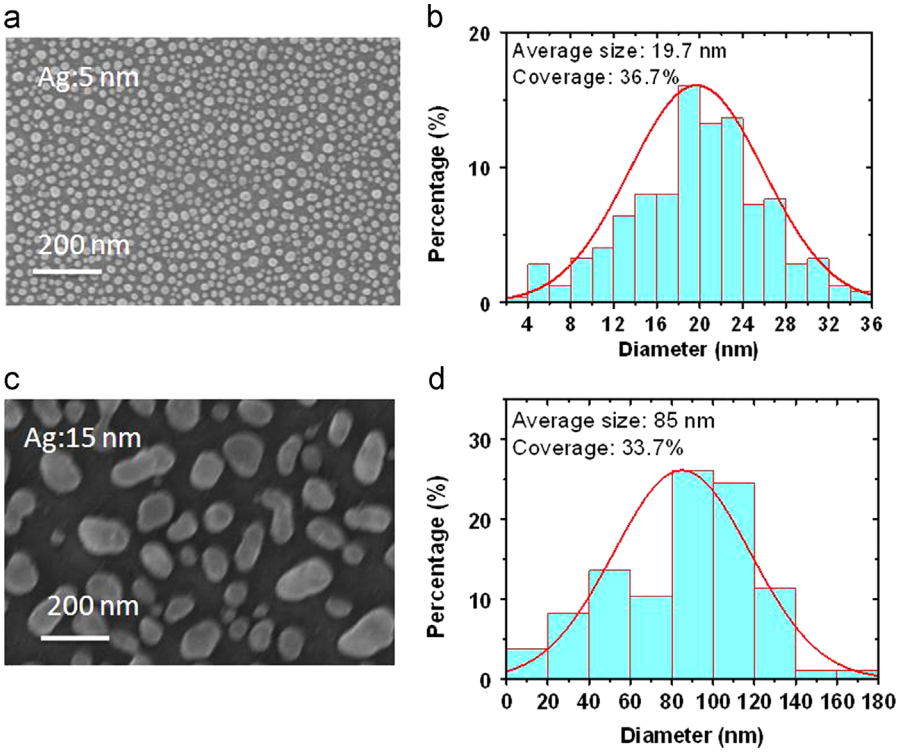

Fig. 2. SEM images and extracted size distributions of Ag NPs formed by (a,b) a 5-nm-thick and (c,d) a 15-nm-thick Ag thin film.

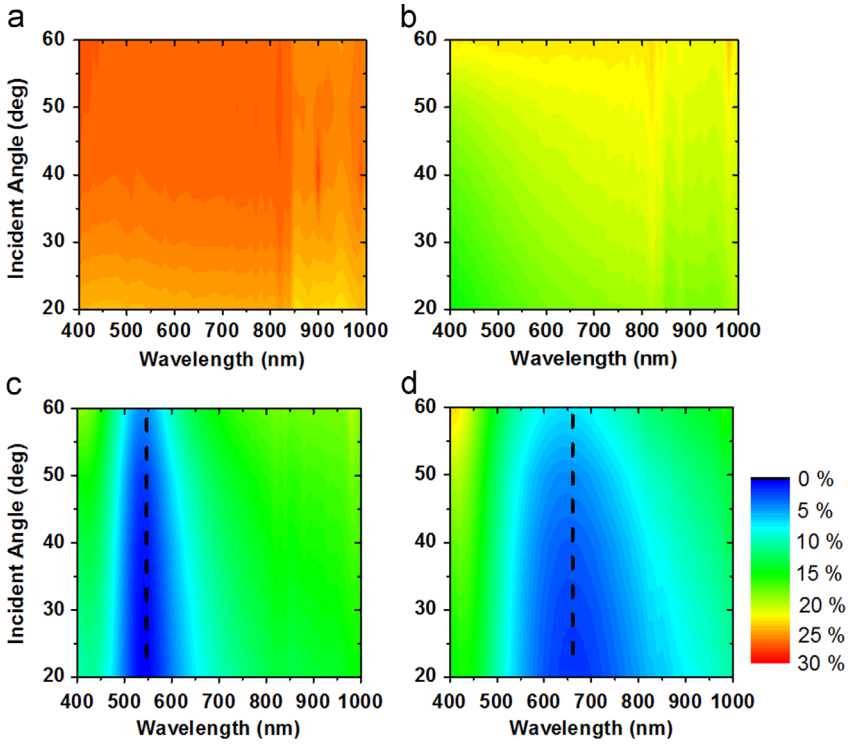

Fig. 3. (a–d) The measured angle-dependent reflectance spectra for four different devices, including (a) a reference cell without any NPs or spacer layer, (b) a cell with a spacer layer only, and two cells with NPs formed by (c) a 5-nm-thick and (d) a 15-nm-thick Ag thin film.

The significant J_{sc} enhancement of 43.7% is contributed by the broadband optical absorption enhancement and the desired absorption peak at ~650 nm where the irradiance is the highest in the solar spectrum [24]. According to the measured *J–V* characteristics shown in Fig. 5, the overall power conversion efficiency (PCE) of this cell was increased from 2.5% to 4.5%, with a J_{sc} of 19.74 mA/cm^2 and an open-circuit voltage (V_{oc}) of 0.39 V. Although the device structure of the solar cell employed in our study has not been optimized, the PCE enhancement with a factor of 80% reveals the promising potential to enhance the optical absorption and the device performance using metallic NPs.

To further reveal the actual enhancement effect of Ag NPs on optical and electrical performance of solar cells, we now analyze two parameters, i.e., the maximum carrier generation rate G_{max} inside the Si active layer and the carrier collection probability $P(E, T)$. As shown in Fig. 6(a), the dependence of the net photocurrent density, J_{ph}, on the effective voltage (V_{eff}) of our reference cell (i.e., sample 1) and the best plasmonic cell (i.e., sample 4) are plotted, where J_{ph} is determined by

$$J_{ph} = J_L - J_D \quad (1)$$

here J_L and J_D are current densities under illumination and dark conditions, respectively. V_{eff} is determined by

$$V_{eff} = V_0 - V_a, \quad (2)$$

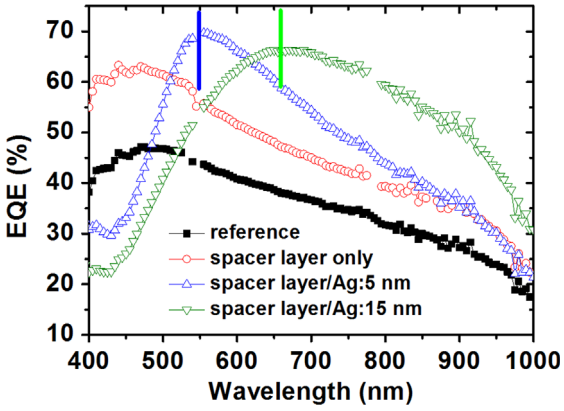

Fig. 4. The measured EQE spectra for the four different devices.

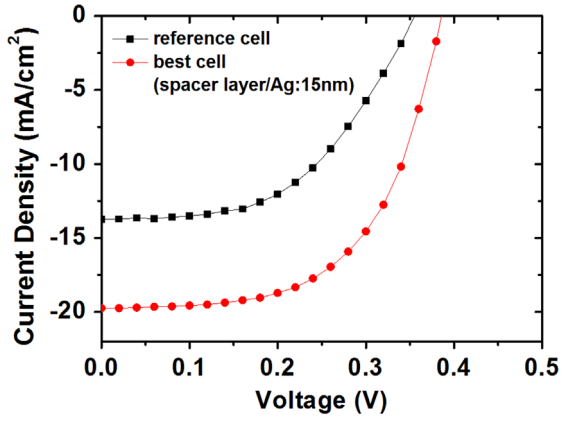

Fig. 5. *J–V* characteristics of the reference cell and the best cell we obtained with a spacer layer and Ag NPs formed by a 15-nm-thick Ag thin film.

where V_0 is the voltage when $J_{ph}=0$ and V_a is the applied voltage [25]. In this way, V_{eff} corresponds to the internal electric field in the device [26]. As shown in Fig. 6(a), J_{ph} increases in the low V_{eff} region first and then becomes saturated at a high V_{eff} value. Due to the sufficiently high electric field in the high V_{eff} region, all photogenerated electron–hole pairs can be assumed to be separated into free carriers [25] and collected by electrodes without recombination [27]. Therefore, the saturation current density (J_{sat}) is limited by the total amount of absorbed incident photons only. G_{max} can be obtained by

$$J_{sat} = qG_{max}(L+W) \quad (3)$$

where q is the electronic charge, L is the carrier diffusion length and W is the space charge region width [28,29]. In our experiment, all Si-based Schottky solar cells were fabricated on the same Si substrate with the same Schottky contact metal (i.e., Cr). Therefore the G_{max} can be determined qualitatively from the observed J_{sat}, which is independent of the applied bias. A larger J_{sat} value corresponds to a higher G_{max}. As shown in Fig. 6(a), the J_{sat} of the plasmonic cell (sample 4) is approximately 198 A m^{-2}, which is 29.3% higher than that of the reference cell (sample1, $J_{sat}=\sim$140 A m^{-2}). Because the value of G_{max} is a measure of the maximum number of photons absorbed [30,31], this enhanced G_{max} confirmed the increased light absorption in the plasmonic device. In the next paragraph, we compare the carrier collection probabilities of these two devices to demonstrate that the extra Ag NPs did not degrade the electrical performance of the devices.

In practical solar cells, only a portion of photogenerated carriers can be collected and contribute to the photocurrent due to the recombination processes. As a result, J_{ph} can be described as

$$J_{ph} = qG_{max}(L+W)P(E, T), \quad (4)$$

where $P(E, T)$ is carrier collection probability (related to the electric field (E) and temperature (T)), representing the portion of the carriers that can be collected by electrodes [29,32,33]. It was predicted that extra metal NPs in the active layers or on the surfaces of photovoltaic devices may function as charge carrier recombination centers which is a loss mechanism for the electric performance although the optical absorption can be enhanced [10,34]. By taking the ratio of Eqs. (4) and (3), we can compare $P(E, T)$ of our devices (i.e., J_{ph}/J_{sat}) as a function of V_{eff} [25,33], as shown in Fig. 6(b). One can see that the values of $P(E, T)$ under short-circuit condition (i.e., $V_a=0$ V, as indicated by the dashed arrow in Fig. 6(b)) were identical for the reference and plasmonic cells, indicating that introducing Ag NPs did not sacrifice the carrier collection of the plasmonic-enhanced device. In the low V_{eff} region, the $P(E, T)$ values for both cells decreased, indicating that the recombination (e.g., Si/metal interface states and defects) began to dominate the carrier transport due to the lower internal electric field [27]. It was observed that the plasmonic-enhanced

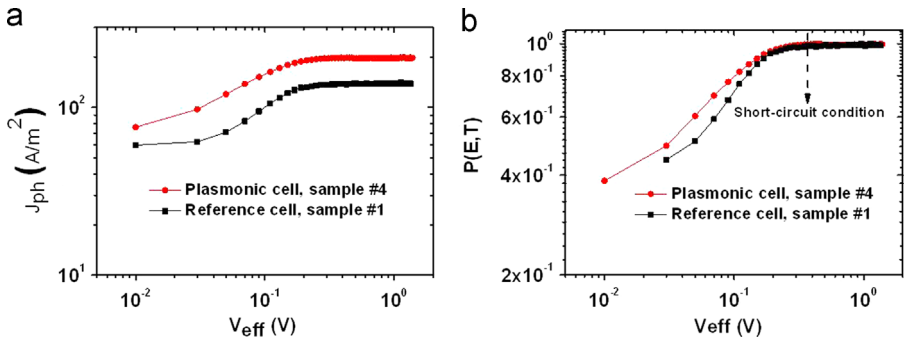

Fig. 6. (a) Photocurrent density (J_{ph}) plotted with respect to effective bias (V_{eff}) for the reference and plasmonic devices. (b) Carrier collection probabilities for the reference and plasmonic devices under short-circuit conditions.

cell showed higher $P(E, T)$ values in the low V_{eff} region. Considering that the plasmonic cell generated more net photocurrent in this region (see Fig. 6(a)), these extra photogenerated carriers can therefore compensate some of the interface states and defects, leading to a higher carrier collection efficiency and also device fill factor [27]. Thus, these additional Ag NPs increased the carrier generation rate in the active layer without degrading electrical properties, thereby enhancing the photocurrent of the solar cell devices.

4. Conclusion

In summary, we demonstrate the positive and tunable effects of Ag NPs in Si-based MIS Schottky barrier solar cells. By controlling the size, shape and distribution of Ag NPs, the optical absorption of the Si absorber layer can be tuned and enhanced without sacrificing the device electrical properties. The best plasmonic cell obtained in this work achieved a power conversion efficiency improvement from 2.5% to 4.5%, with a photocurrent enhancement of 43.7%.

According to previous theoretical predictions, an enhancement factor of ~40% for optical absorption and photocurrent was reported by carefully designing metallic nanostructures on dielectric spacer layers (e.g., SiO_2 or SiN_x) [35,36]. However, photocurrent enhancements of 6% and 19% were experimentally realized for Si solar cells by introducing Ag or Au NPs [11,15]. In this paper, we reported an enhancement of 43.7% in photocurrent, which is comparable with previously reported theoretical results and higher than experimental results on Si solar cells. This enhancement is attributed to a combination effect of the surface reflectance reduction due to the dielectric spacer layer and the light-trapping effect contributed by Ag nanoparticles. The proposed design principle and analysis is quite general and will be suitable for other types of optoelectronic devices, such as thin-film solar cells [9,10] and photodetectors [37].

Acknowledgments

C. Tong, J. Yun and W. Anderson gratefully acknowledge the support from the US Air Force Office of Scientific Research (FA95501010154) with Dr. Kitt Reinhardt and Dr. James Hwang as supervisors. H. Song and Q. Gan acknowledge funding support from National Science Foundation (Grant no. ECCS1128086).

References

[1] D.L. Pulfrey, Mis solar-cells – review, IEEE Trans. Electron. Dev. 25 (1978) 1308–1317.
[2] R.B. Godfrey, M.A. Green, 655-Mv open-circuit voltage, 17.6-percent efficient silicon Mis solar-cells, Appl. Phys. Lett. 34 (1979) 790–793.
[3] W.A. Anderson, A.E. Delahoy, J.K. Kim, S.H. Hyland, S.K. Dey, High-efficiency Cr-Mis solar-cells on single and polycrystalline silicon, Appl. Phys. Lett. 33 (1978) 588–590.
[4] J.I.B. Wilson, J. Mcgill, Amorphous-silicon Mis solar-cells, IEE Proc.-I 2 (1978) S7–S10.
[5] D.B. Li, X.J. Sun, H. Song, Z.M. Li, Y.R. Chen, H. Jiang, G.Q. Miao, Realization of a high-performance GaN UV detector by nanoplasmonic enhancement, Adv. Mater. 24 (2012) 845–849.
[6] H.R. Stuart, D.G. Hall, Island size effects in nanoparticle-enhanced photodetectors, Appl. Phys. Lett. 73 (1998) 3815–3817.
[7] S.H. Lim, W. Mar, P. Matheu, D. Derkacs, E.T. Yu, Photocurrent spectroscopy of optical absorption enhancement in silicon photodiodes via scattering from surface plasmon polaritons in gold nanoparticles, J. Appl. Phys. 101 (2007).
[8] S.P. Sundararaian, N.K. Grady, N. Mirin, N.J. Halas, Nanoparticle-induced enhancement and suppression of photocurrent in a silicon photodiode, Nano Lett. 8 (2008) 624–630.
[9] H.A. Atwater, A. Polman, Plasmonics for improved photovoltaic devices, Nat. Mater. 9 (2010) 205–213.
[10] Q.Q. Gan, F.J. Bartoli, Z.H. Kafafi, Plasmonic-enhanced organic photovoltaics: breaking the 10% efficiency barrier, Adv. Mater. 25 (2013) 2385–2396.
[11] S. Pillai, K.R. Catchpole, T. Trupke, M.A. Green, Surface plasmon enhanced silicon solar cells, J. Appl. Phys. 101 (2007).
[12] P. Spinelli, M. Hebbink, R. de Waele, L. Black, F. Lenzmann, A. Polman, Optical impedance matching using coupled plasmonic nanoparticle arrays, Nano Lett. 11 (2011) 1760–1765.
[13] N. Fahim, Z. Ouyang, Y.N. Zhang, B.H. Jia, Z.R. Shi, M. Gu, Efficiency enhancement of screen-printed multicrystalline silicon solar cells by integrating gold nanoparticles via a dip coating process, Opt. Mater. Express 2 (2012) 190–204.
[14] Y.A. Akimov, K. Ostrikov, E.P. Li, Surface plasmon enhancement of optical absorption in thin-film silicon solar cells, Plasmonics 4 (2009) 107–113.
[15] N.F. Fahim, Z. Ouyang, B.H. Jia, Y.A. Zhang, Z.R. Shi, M. Gu, Enhanced photocurrent in crystalline silicon solar cells by hybrid plasmonic antireflection coatings, Appl. Phys. Lett. 101 (2012).
[16] X. Chen, B.H. Jia, J.K. Saha, B.Y. Cai, N. Stokes, Q. Qiao, Y.Q. Wang, Z.R. Shi, M. Gu, Broadband enhancement in thin-film amorphous silicon solar cells enabled by nucleated silver nanoparticles, Nano Lett. 12 (2012) 2187–2192.
[17] T. Kume, S. Hayashi, H. Ohkuma, K. Yamamoto, Enhancement of photoelectric conversion efficiency in copper phthalocyanine solar cell: White light excitation of surface plasmon polaritons, Jpn. J. Appl. Phys. 1 (34) (1995) 6448–6451.
[18] M. Westphalen, U. Kreibig, J. Rostalski, H. Luth, D. Meissner, Metal cluster enhanced organic solar cells, Sol. Energy Mater. Sol. C 61 (2000) 97–105.
[19] F.J. Beck, A. Polman, K.R. Catchpole, Tunable light trapping for solar cells using localized surface plasmons, J. Appl. Phys. 105 (2009).
[20] D.M. Schaadt, B. Feng, E.T. Yu, Enhanced semiconductor optical absorption via surface plasmon excitation in metal nanoparticles, Appl. Phys. Lett. 86 (2005).
[21] C. Tong, J. Yun, E. Kozarsky, W.A. Anderson, Nanoplasmonic Enhanced ZnO/Si heterojunction metal–semiconductor–metal photodetectors, J. Electron. Mater. 42 (2013) 889–893.
[22] T.L. Temple, G.D.K. Mahanama, H.S. Reehal, D.M. Bagnall, Influence of localized surface plasmon excitation in silver nanoparticles on the performance of silicon solar cells, Sol. Energy Mater. Sol. C 93 (2009) 1978–1985.
[23] C. Hagglund, M. Zach, G. Petersson, B. Kasemo, Electromagnetic coupling of light into a silicon solar cell by nanodisk plasmons, Appl. Phys. Lett. 92 (2008).
[24] Y.A. Akimov, W.S. Koh, Design of plasmonic nanoparticles for efficient subwavelength light trapping in thin-film solar cells, Plasmonics 6 (2011) 155–161.
[25] L.Y. Lu, Z.Q. Luo, T. Xu, L.P. Yu, Cooperative plasmonic effect of Ag and Au nanoparticles on enhancing performance of polymer solar cells, Nano Lett. 13 (2013) 59–64.
[26] L.J.A. Koster, E.C.P. Smits, V.D. Mihailetchi, P.W.M. Blom, Device model for the operation of polymer/fullerene bulk heterojunction solar cells, Phys. Rev. B 72 (2005).
[27] Z.C. He, C.M. Zhong, X. Huang, W.Y. Wong, H.B. Wu, L.W. Chen, S.J. Su, Y. Cao, Simultaneous enhancement of open-circuit voltage, short-circuit current density, and fill factor in polymer solar cells, Adv. Mater. 23 (2011) 4636–4643.
[28] A. Goetzberger, J. Knobloch, B. Voss, Crystalline Silicon Solar Cells, Wiley, Chichester New York, 1998.
[29] P. Bhattacharya, Semiconductor optoelectronic devices, 2nd ed., Prentice Hall, Upper Saddle River, NJ, 1997.
[30] Y.Y. Liang, Z. Xu, J.B. Xia, S.T. Tsai, Y. Wu, G. Li, C. Ray, L.P. Yu, For the bright future-bulk heterojunction polymer solar cells with power conversion efficiency of 7.4%, Adv. Mater. 22 (2010) E135–E138.
[31] C.C.D. Wang, W.C.H. Choy, C.H. Duan, D.D.S. Fung, W.E.I. Sha, F.X. Xie, F. Huang, Y. Cao, Optical and electrical effects of gold nanoparticles in the active layer of polymer solar cells, J. Mater. Chem. 22 (2012) 1206–1211.
[32] V.D. Mihailetchi, H.X. Xie, B. de Boer, L.J.A. Koster, P.W.M. Blom, Charge transport and photocurrent generation in poly (3-hexylthiophene): methanofullerene bulk-heterojunction solar cells, Adv. Funct. Mater. 16 (2006) 699–708.
[33] J.L. Wu, F.C. Chen, Y.S. Hsiao, F.C. Chien, P.L. Chen, C.H. Kuo, M.H. Huang, C.S. Hsu, Surface Plasmonic Effects of metallic nanoparticles on the performance of polymer bulk heterojunction solar cells, ACS Nano 5 (2011) 959–967.
[34] V.E. Ferry, J.N. Munday, H.A. Atwater, Design considerations for plasmonic photovoltaics, Adv. Mater. 22 (2010) 4794–4808.
[35] Y.N. Zhang, Z. Ouyang, N. Stokes, B.H. Jia, Z.R. Shi, M. Gu, Low cost and high performance Al nanoparticles for broadband light trapping in Si wafer solar cells, Appl. Phys. Lett. 100 (2012).
[36] R.A. Pala, J. White, E. Barnard, J. Liu, M.L. Brongersma, Design of plasmonic thin-film solar cells with broadband absorption enhancements, Adv. Mater. 21 (2009) 3504–3509.
[37] G. Konstantatos, E.H. Sargent, Nanostructured materials for photon detection, Nat. Nanotechnol. 5 (2010) 391–400.